https://doi.org/10.31436/iiumej.v27i3.4187

Optimal Operating Cost for a Grid-connected Microgrid Using Quadratic Interpolation Optimization

THACH CHI PHAN [1], THUAN THANH NGUYEN[1*], THANG TRUNG NGUYEN [2]

[1] *Faculty of Electrical Engineering Technology, Industrial University of Ho Chi Minh City, Ho Chi Minh City, Vietnam.*
[2] *Power System Optimization Research Group, Faculty of Electrical and Electronics Engineering, Ton Duc Thang University, Ho Chi Minh City, Vietnam.*

**Corresponding author: nguyenthanhthuan@iuh.edu.vn*

(Received: 3 February 2026; Accepted: 10 May 2026; Published online: 11 September 2026)

ABSTRACT: This study applies the Quadratic Interpolation Optimization Method (QIOM) to minimize the operating cost of a grid-connected MG over a 24-hour horizon. This optimization-based scheduling framework actively controls the diesel generator (DG) and battery energy storage system (BESS). In contrast, renewable sources such as solar and wind are treated as fixed inputs. Three operating scenarios are examined to assess the roles of the controllable generator and the BESS. The findings indicate that cost reduction mainly depends on how energy flows are coordinated over time, rather than on the total energy exchanged. The BESS plays a key role by shifting energy from low-load periods to peak-load periods, which improves overall economic performance. QIOM is also compared with Particle Swarm Optimization (PSO), Gravitational Search Algorithm (GSA), Grey Wolf Optimizer (GWO), and Heap-Based Optimization (HBO) in terms of solution quality, robustness, and computational performance. The comparative results demonstrate that QIOM achieves lower operating costs and more consistent performance across 20 independent runs. The Wilcoxon signed-rank test confirms that these improvements are statistically significant. However, this performance gain comes at the cost of increased computational time. Therefore, QIOM is more suitable for offline scheduling applications.

ABSTRAK: Kajian ini menggunakan Kaedah Pengoptimuman Interpolasi Kuadratik (QIOM) bagi meminimum kos operasi MG yang disambung ke grid selama 24 jam. Kajian ini mencadangkan penjadualan optimum di mana penjana diesel (DG) dan sistem storan tenaga bateri (BESS) dikawal secara aktif. Sebaliknya, sumber boleh diperbaharui seperti solar dan angin dianggap sebagai input tetap. Tiga senario operasi diperiksa bagi menilai peranan penjana boleh kawal dan BESS. Dapatan menunjukkan bahawa pengurangan kos bergantung pada pelarasan aliran tenaga dari semasa ke semasa, bukan pada jumlah penukaran tenaga. BESS memainkan peranan penting dengan mengalihkan tenaga dari tempoh beban rendah kepada tempoh beban puncak, ini meningkatkan prestasi ekonomi keseluruhan. Perbandingan QIOM dengan Pengoptimuman Kawanan Partikel (PSO), Algoritma Carian Graviti (GSA), Pengoptimum Serigala Kelabu (GWO), dan Pengoptimum Berasas Timbunan (HBO) turut dilakukan dari segi kualiti penyelesaian, kekukuhan dan prestasi pengiraan. Dapatan kajian menunjukkan bahawa QIOM mencapai kos operasi lebih rendah dengan prestasi konsisten merentasi 20 larian bebas. Ujian pangkat Wilcoxon mengesahkan bahawa penambahbaikan ini adalah signifikan secara statistik. Walau bagaimanapun, peningkatan prestasi ini datang dengan kos lebih tinggi daripada masa pengiraan. Oleh itu, QIOM lebih sesuai untuk aplikasi penjadualan luar talian.

KEYWORDS: *Battery energy storage system, Metaheuristic optimization, Microgrid scheduling, Quadratic Interpolation Optimization, Temporal energy shifting*

https://doi.org/10.31436/iiumej.v27i3.4187

1. INTRODUCTION

Microgrids (MGs) have become a promising solution for integrating distributed energy resources, including photovoltaic (PV) systems, wind turbines (WT), DG, and BESS, into conventional power systems. By enabling local power generation and flexible operation, MGs improve system resilience, reduce transmission losses, and support the transition to low-carbon energy systems [1-3]. In particular, grid-connected MGs provide an efficient platform for coordinating renewable power generation with conventional sources while maintaining a reliable power supply.

However, the growing penetration of renewable energy sources introduces major operational challenges because of their intermittent characteristics. Changes in solar radiation, wind speed, and load demand complicate operational planning, leading to power imbalances and higher operating costs [4-8]. Recent studies highlight the importance of planning frameworks that account for these uncertainties in practical MG operations, especially under real-time variable electricity tariffs [9, 10]. To address these issues, BESS is widely integrated into MGs to provide energy buffers, reduce peak loads, and improve operational flexibility. However, coordinating multiple energy sources under time-varying conditions remains a challenging optimization task, especially in systems with nonlinear constraints and multidimensional decision spaces. The system's dynamic behavior increases operational complexity, making conventional methods unreliable and ineffective [11].

Metaheuristic methods are widely used in MG power management. PSO is one of the most common options. It is easy to implement and performs well in nonlinear problems. Its applications include MG planning, battery operation under uncertainty [11, 12], and reactive power dispatch with complex constraints. For independent MGs, hybrid PSO–GSA approaches have been used for frequency tuning [13]. GSA alone also performs well in PV-based MG optimization [14]. Even so, PSO has limitations. Performance can vary depending on parameter settings, and early convergence may still occur. This issue becomes more evident in high-dimensional or multimodal problems [15, 16]. These challenges are more pronounced in multi-phase MG optimization. The interaction of variables over time adds complexity. As a result, PSO may lose effectiveness under such conditions. However, most existing methods focus on minimizing total cost, while the temporal coordination of energy flows is often overlooked.

In parallel, nature-inspired artificial intelligence algorithms are emerging. The GWO algorithm demonstrates robust performance in complex MG optimization problems due to its balanced discovery-exploitation mechanism [17-20]. Similarly, the HBO algorithm improves convergence and reduces sensitivity to initial conditions in energy management problems [21-23]. This makes these methods suitable for complex MG optimization problems.

Despite the advantages, several limitations remain. Many methods still suffer from premature convergence, sensitivity to parameter adjustments, and reduced performance in problems with many constraints [24]. For example, PSO-based methods are sensitive to parameter settings such as inertial weights and acceleration coefficients, which can significantly affect convergence behavior. They can also converge prematurely and get stuck at local optimal points in the multimodal search space [15]. Most studies focus on minimizing total operating costs, while the temporal characteristics of energy exchange receive less attention. The timing of energy input and output is crucial because electricity prices and renewable energy generation profiles vary over time. Recent studies indicate that planning performance depends not only on the amount of energy exchanged but also on its timing [25, 26]. To address these limitations, this paper investigates applying QIOM, a derivative-free optimization technique [24], to minimize the operating costs of grid-connected MGs [27].

https://doi.org/10.31436/iiumej.v27i3.4187

Unlike conventional metaheuristic algorithms, QIOM uses an interpolation-based search mechanism that balances global exploration and local exploitation without requiring gradient information. This method is evaluated using real-world meteorological data from Ho Chi Minh City, Vietnam, including solar radiation, wind speed, and temperature [28, 29]. This provides a more realistic assessment of its practical performance.

The main contributions of this study are summarized as follows:

1) A scenario-based optimization framework is developed to analyze MG operation under three practical configurations. It enables a clearer assessment of the roles of DG and BESS.
2) A consistent evaluation protocol is adopted using 20 independent runs. The mean and standard deviation are reported, and the Wilcoxon signed-rank test is used to compare algorithms.
3) The findings show that cost reduction is mainly driven by the coordination of energy flows over time, rather than the total energy exchanged.
4) The QIOM-based approach, which relies on interpolation without gradient information, is validated using real-world data from Ho Chi Minh City, showing competitive performance under practical operating conditions.

The remainder of this paper is organized as follows. Section 2 presents the system model and problem formulation. Section 3 describes the QIOM-based optimization method and its application to efficient MG scheduling. Section 4 discusses the simulation results, while Section 5 concludes the paper.

2. Microgrid Model and Problem Formulation

Fig. 1 illustrates the structure of the MG system considered in this study. The system comprises four main components: a solar PV farm, a wind power farm, a DG, and a BESS. These energy sources collectively supply electricity to meet the demand profile, which follows a typical 24-hour load curve as depicted in Fig. 2.

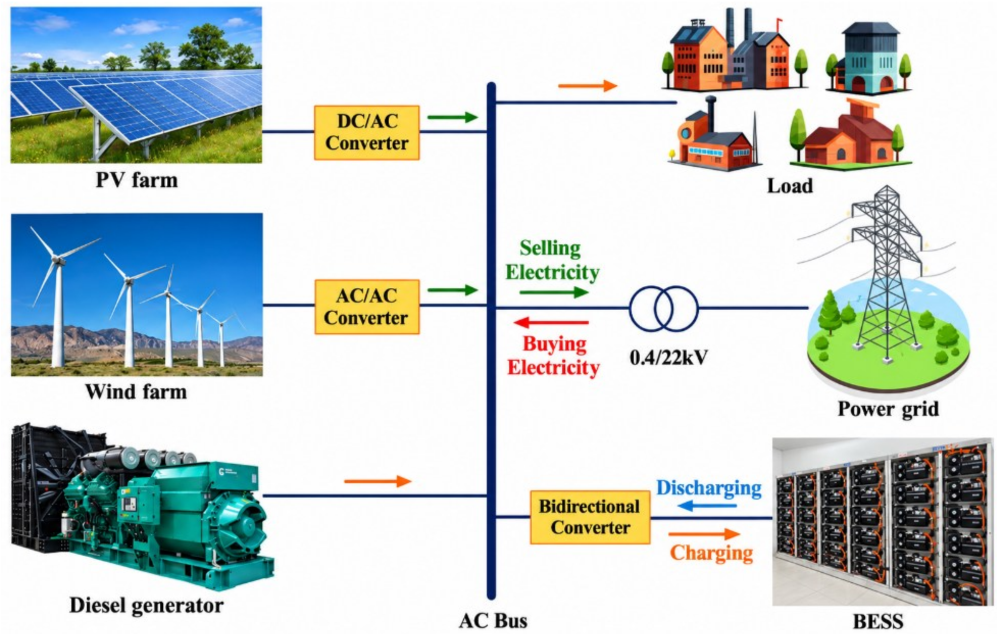

Figure 1. Configuration and energy flow structure of the proposed grid-connected MG.

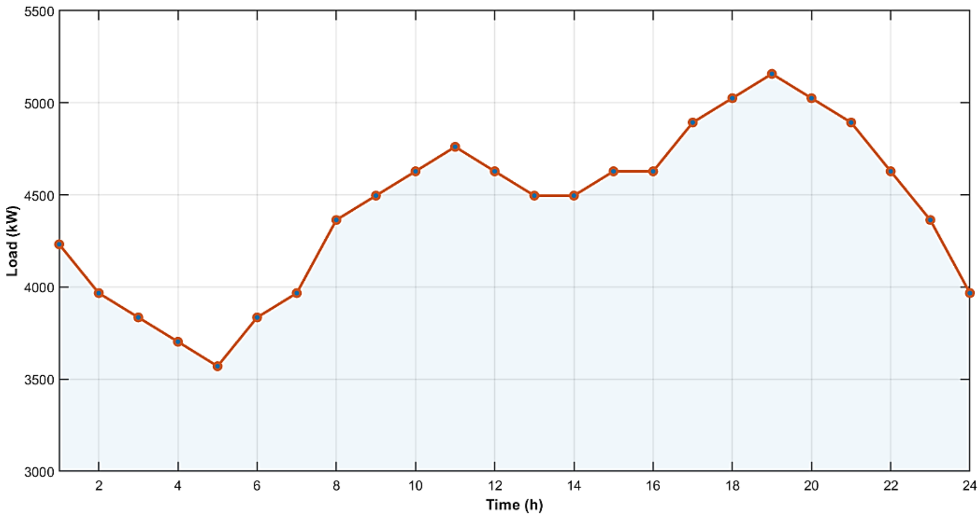

Figure 2. Typical 24-hour load demand profile used in the case study.

2.1. Photovoltaic farm

The PV farm in the MG is designed with a rated capacity of 2500 kW. The direct current (DC) output from the PV is converted to alternating current (AC) via an inverter and then fed into the AC bus. The actual power output at time *t*, denoted as $P_{PV}(t)$, mainly depends on solar irradiance and the operating temperature of the PV modules. The output power is estimated using the following Eq. (1) [30-32]:

$$P_{PV}(\mathrm{t}) = P_{STC} \times (G(t)/1000) \times (1-\alpha(T_{PV}(t)-25)) \times \eta_{PV} \tag{1}$$

where: P_{STC} is the rated power under standard test conditions; $G(t)$ and $T_{PV}(t)$ represent the solar irradiance and PV module temperature at time *t*, respectively, while α denotes the temperature coefficient; and η_{PV} represents the DC/AC converter efficiency.

2.2. Wind farm

The wind farm consists of eight WTs with a combined rated capacity of 4000 kW. The electrical output from the WTs is converted to AC and delivered to the main AC bus via a power electronic converter. The actual power output at time t, denoted as $P_{WT}(t)$, is highly dependent on the wind speed and is calculated using the following expression given by Eq. (2) [33]:

$$P_{WT}(\mathrm{t}) = \mathrm{N}_{TB} \times \eta_{\_\mathrm{W}} \times \begin{cases} 0, \mathrm{V}_t(\mathrm{t}) < \mathrm{V}_{\mathrm{cut\_in}} \\ P_n\left(\dfrac{\mathrm{V}_t(\mathrm{t}) - \mathrm{V}_{\mathrm{cut\_in}}}{\mathrm{V}_{\mathrm{r}} - \mathrm{V}_{\mathrm{cut\_in}}}\right)^3, \mathrm{V}_{\mathrm{cut\_in}} < \mathrm{V}_t(\mathrm{t}) < \mathrm{V}_{\mathrm{r}} \\ P_n, \mathrm{V}_{\mathrm{r}} < \mathrm{V}_t(\mathrm{t}) < \mathrm{V}_{\mathrm{cut\_out}} \end{cases} \tag{2}$$

where: N_{TB} is the number of WTs in the system; $\eta_{\_W}$ is the AC/AC converter efficiency; $V_t(t)$ is the wind speed at time t; V_r is the rated wind speed; P_n is the power of one WT; V_{cut_in} and V_{cut_out} are the cut-in and cut-out wind speeds.

The input data used in this study include solar irradiance, ambient temperature [28], and wind speed [29], as shown in Fig. 3. These data represent a typical dry-season day in Ho Chi Minh City, Vietnam.

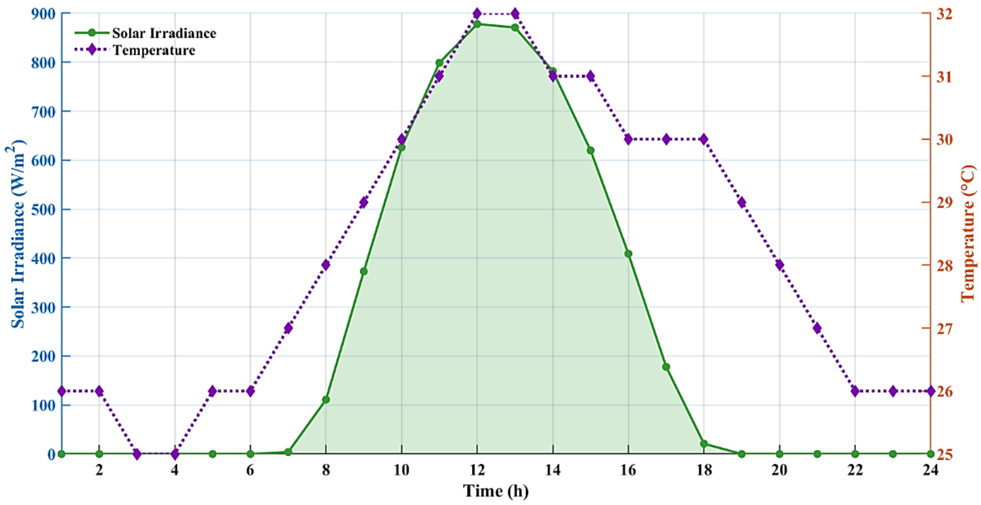

Figure 3. Solar irradiance and ambient temperature profiles for a typical dry-season day.

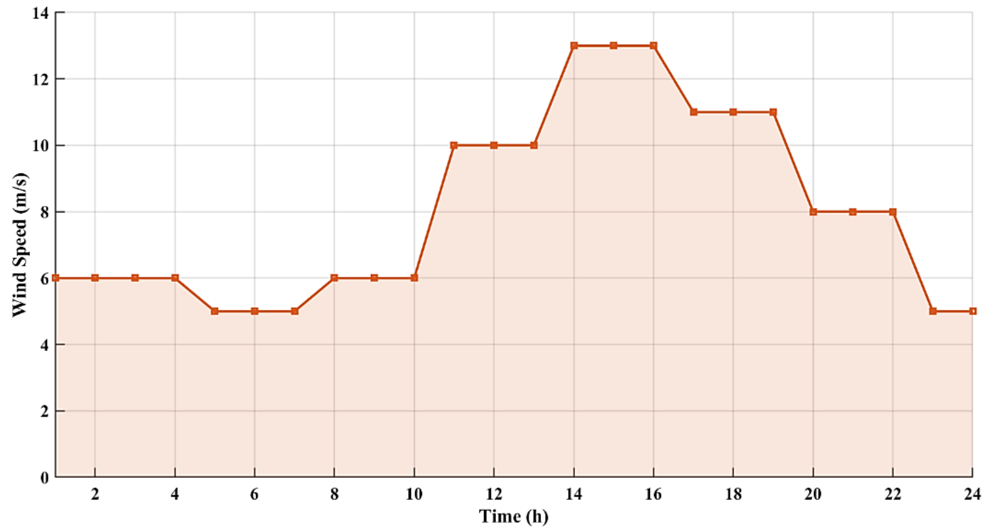

Figure 4. Wind speed profile for a typical dry-season day.

2.3. Diesel generator system

The DG has a capacity of 1750 kW, and its operating cost is determined by fuel consumption and fuel cost. This cost is calculated using Eq. (3) [34]:

$$C_{DG\_OP}(t) = C_{diesel} \times \left(A_{DG} + B_{DG} \times P_{DG}(t) + C_{DG} \times P^2_{DG}(t) \right) \tag{3}$$

Where: A_{DG}, B_{DG}, and C_{DG} represent the coefficients that influence the fuel consumption of the DG, and C_{diesel} is the diesel fuel cost ($/gal). The coefficient values are in Table 1.

Table 1. Coefficient values related to the DG [4].

Coefficients	Values
A_{DG}	22.9 (gal/h)
B_{DG}	0.0280 (gal/kWh)
C_{DG}	1.849×10^{-5} (gal/kWh)^2
C_{diesel}	2.258 ($/gal)

The DG system's power output at time t, denoted as $P_{DG}(t)$, must operate within predefined minimum and maximum limits, as expressed in Eq. (4).

$$P_{DG\_min} \leq P_{DG}(t) \leq P_{DG\_max} \tag{4}$$

2.4. Battery energy storage system (BESS)

The BESS, with a total capacity of 4600 kWh, operates in both charging and discharging modes. It is connected to the AC bus through a bidirectional converter, enabling two-way energy exchange.

At any time t, the BESS power output/input, denoted as $P_{BESS}(t)$, is subject to operational constraints to ensure safe and efficient operation. These constraints can be expressed as follows:

$$-P_{\text{BESS}\_max} \leq P_{\text{BESS}}(t) \leq P_{\text{BESS}\_max} \tag{5}$$

where: P_{BESS_max} denotes the maximum discharging power (kW) that the BESS can supply to the MG, while - P_{BESS_max} represents the maximum charging power.

The energy stored in the BESS at time t, represented as $E_{BESS}(t)$, is calculated using Eq. (6) [4].

$$E_{BESS}(\text{t}) = \begin{cases} E_{BESS}(\text{t}-1) - \dfrac{\Delta T \times P_{BESS}(\text{t})}{\eta_{\_d}}, P_b(\text{t}) > 0 \\ E_{BESS}(\text{t}-1) - \Delta T \times \eta_{\_c} \times P_{BESS}(\text{t}), P_{BESS}(\text{t}) \leq 0 \end{cases} \tag{6}$$

where: $\eta_{\_c}$ and $\eta_{\_d}$ denote the charging and discharging efficiencies of the BESS, respectively, and ΔT is the sampling time (1 hour).

The BESS state of charge (SOC) is determined using Eq. (7).

$$SOC(\text{t}) = \frac{E_{BESS}(\text{t})}{B_{capacity}} \tag{7}$$

where: $B_{capacity}$ denotes the energy capacity of the BESS (kWh).

To ensure battery longevity, the SOC must be maintained within predefined minimum and maximum limits, as expressed in Eq. (8).

$$SOC_{min} \leq SOC(t) \leq SOC_{max} \tag{8}$$

For operational continuity, the battery SOC is constrained to reach 50% at the end of the 24-hour cycle, ensuring energy availability for the subsequent day.

The BESS operating cost function is given by the following expression [35]:

$$C_{BESS\_op}(\text{t}) = \frac{C_{BESS} \times \eta_{\_c} \times \Delta T \times P_{BESS\_ch}(\text{t})}{2 \times N_{cycle}} + \frac{C_{BESS} \times \Delta T \times P_{BESS\_\text{dis}}(\text{t})}{2 \times \eta_{\_d} \times N_{cycle}} + C_{\deg} \times P_{BESS}(\text{t}) \tag{9}$$

where: $P_{BESS}(t)$ denotes the total power of the BESS at time t, $P_{BESS\_ch}(t)$ and $P_{BESS\_dis}(t)$ denote the charging and discharging power at time t, respectively; C_{BESS} refers to the investment cost of the BESS (\$/kWh), N_{cycle} is the number of cycles corresponding to the battery's lifespan, and C_{deg} is the degradation cost coefficient, representing the penalty associated with battery aging.

2.5. Power grid

A 5 MVA, 0.4/22 kV transformer facilitates power transfer between the MG and the utility grid, subject to transmission and stability constraints as expressed in Eq. (10).

$$P_{Utility\_\min} \leq P_{Utility}(t) \leq P_{Utility\_\max} \tag{10}$$

where: PUtility(t) denotes the power exchanged between the main grid and the MG at time t.

A positive value of PUtility(t)>0 indicates that power is imported from the grid to the MG, while a negative value PUtility(t)<0 indicates that power is exported from the MG to the grid.

The power transferred from the grid to the MG at time t is given as:

$$P_{Utility}(t) = P_{Load}(t) - P_{PV}(t) - P_{WT}(t) - P_{BESS}(t) - P_{DG}(t) \tag{11}$$

where: $P_{Load}(t)$ denotes the load power at time t, following the load curve shown in Fig. 2.

2.6. Objective function

The objective of the proposed optimization model is to minimize the MG's total operating cost over a 24-hour period. This objective is formulated through a fitness function, which serves as the performance metric for evaluating candidate solutions. The objective function can be formulated as follows:

$$Min\, C_{op\_MG} = \sum_{t=1}^{24}\left(C_{MG\_buy} + C_{MG\_sell} + C_{B\_\mathrm{op}} + C_{DG\_\mathrm{op}}\right) \tag{12}$$

where: C_{MG_buy} denotes the cost of purchasing electricity from the grid ($), while C_{MG_sell} represents the revenue obtained from selling electricity to the grid ($). These values are determined by Eq. (13) and Eq. (14):

$$C_{MG\_buy} = T_{buy}(t) \times P_{Utility}(t) \ , \ P_{Utility}(t) > 0 \tag{13}$$

$$C_{MG\_sell} = T_{sell}(t) \times P_{Utility}(t) \ , \ P_{Utility}(t) < 0 \tag{14}$$

where: $T_{buy}(t)$, $T_{sell}(t)$ represent the electricity procurement and sale tariffs at time t, as shown in Table 2.

Table 2. Time-based electricity prices for cost optimization modeling [4].

Type of tariff	Time	Value ($/kWh)
Purchasing	00:00 – 7:00	0.06
	8:00 – 16:00	0.144
	17:00 – 20:00	0.252
	21:00 – 00:00	0.144
Selling	All day	0.0582

3. Optimizing The Operating Cost of MG System Using Quadratic Interpolation Optimization Method

QIOM is a mathematically driven algorithm that leverages quadratic interpolation through three points to locate a function's minimum. It has demonstrated effectiveness in numerous optimization problems, particularly in curve-based search strategies [24, 36-37].

3.1. Quadratic Interpolation Method

Let $q(x)$ be a quadratic function defined as an approximation of the objective function *f(x)*. By identifying the minimum point of *q(x)*, an approximate minimum of *f(x)* can be obtained. The quadratic function is defined as:

$$q(x) = ax^2 + bx + c, \text{ with } a, b, c \in R \tag{15}$$

Assume that the function *f(x)* is known at three distinct points $P_i(x_i, f(x_i))$, $P_j(x_j, f(x_j))$, and $P_k(x_k, f(x_k))$, where $a \le x_i < x_j < x_k \le b$. The quadratic approximation $q(x)$ satisfies the interpolation conditions at these points:

$$\begin{cases} q(x_i) = ax_i^2 + bx_i + c = f(x_i) \\ q(x_j) = ax_j^2 + bx_j + c = f(x_j) \\ q(x_k) = ax_k^2 + bx_k + c = f(x_k) \end{cases} \tag{16}$$

By differentiating Eq. (15) and setting the derivative to zero, the minimum point of the parabola is found as:

$$x_{\min} = -\frac{b}{2a} \tag{17}$$

Alternatively, the minimum can also be calculated using the following expression derived from Newton's divided differences:

$$x_{\min} = \frac{1}{2}(x_i + x_j) + \frac{1}{2}\frac{(f(x_i) - f(x_j))(f(x_j) - f(x_k))(f(x_k) - f(x_i))}{(x_j - x_k)f(x_i) + (x_k - x_i)f(x_j) + (x_i - x_j)f(x_k)} \tag{18}$$

The interpolation function $q(x)$ can also be constructed explicitly using the Lagrange interpolation formula:

$$q(x) = \frac{(x - x_j)(x - x_k)}{(x_i - x_j)(x_i - x_k)} f(x_i) + \frac{(x - x_i)(x - x_k)}{(x_j - x_i)(x_j - x_k)} f(x_j) + \frac{(x - x_i)(x - x_j)}{(x_k - x_i)(x_k - x_j)} f(x_k) \tag{19}$$

Once x_{min} is found, a new triplet is formed around it to define a smaller search region. Quadratic interpolation is then repeated iteratively until a convergence criterion or target accuracy is reached, yielding the final approximate minimum.

3.2. Quadratic Interpolation Optimization Method

The QIOM consists of two main phases, namely exploration and exploitation, as illustrated in Fig. 5. The algorithm starts by initializing parameters and generating a random population of candidate solutions. After evaluating the objective function, the best solution is returned if the stopping criterion is met; otherwise, the iterative optimization process continues.

At each iteration, two candidate solutions are randomly selected from the population. Let $rando \sim U(0,1)$ be a control random variable used to probabilistically determine the search phase. If $rando > 0.5$, the Generalized Quadratic Interpolation (GQI) function is computed based on the current solution and the two selected individuals Eq. (20), followed by the exploration phase Eq. (21). Otherwise, the GQI function is constructed using the best-known solution and two randomly selected individuals Eq. (22), leading to the exploitation phase Eq. (23).

After a new candidate solution is generated, the best solution is selected based on the fitness comparison described in Eq. (24). This iterative process continues until the convergence criterion is met.

3.2.1. Exploration phase

This phase explores the full variable space to avoid local optima and premature convergence. Promising regions are identified by randomly selecting individuals that satisfy the GQI conditions. Positions are updated using Eq. (20) and Eq. (21) [24].

$$x_{\min\_i,rando1,rando2}(\mathrm{t}) = GQI(x_i(\mathrm{t}), x_{rando1}(\mathrm{t}), x_{rando2}(\mathrm{t}), \mathrm{fit}(x_i(\mathrm{t}), \mathrm{fit}(x_{rando1}(\mathrm{t})), \mathrm{fit}(x_{rando2}(\mathrm{t}))) \tag{20}$$

$$v_i(\mathrm{t}+1) = x_{\min\_i,rando1,rando2}(\mathrm{t}) + w_1.(x_{rando3}(\mathrm{t}) - x_{\min\_i,rando1,rando2}(\mathrm{t})) + round(0.5(0.5+r_1))\log\frac{r_2}{r_3} \tag{21}$$

where: x_{rando1}, x_{rando2}, and x_{rando3} represent the positions of selected individuals from the population; r_1, r_2, and r_3 are random numbers uniformly distributed in (0, 1), and fit (.) denotes the fitness function value. The minimizer x_{min} is estimated from the triplet (x_i, fit(x_i)), (x_{rando2}, fit(x_{rando2})) and (x_{rando3}, fit(x_{rando3})) via GQI.

3.2.2. Exploitation phase

This phase enhances the best-known solution through a local search strategy to accelerate convergence toward the global optimum. QIOM randomly selects two individuals from the population and uses the current best solution in the GQI process to generate an improved candidate. The updated position is calculated using Eq. (22) within the defined minimum region [24].

$$x_{\min\_\mathrm{best},rando1,rando2}(\mathrm{t}) = GQI(x_{best}(\mathrm{t}), x_{rando1}(\mathrm{t}), x_{rando2}(\mathrm{t}), \mathrm{fit}(x_{best}(\mathrm{t}), \mathrm{fit}(x_{rando1}(\mathrm{t})), \mathrm{fit}(x_{rando2}(\mathrm{t}))) \tag{22}$$

$$v_i(\mathrm{t}+1) = x_{\min\_i,rando1,rando2}(\mathrm{t}) + w_2.(x_{best}(\mathrm{t}) - round(1+\mathrm{rando}).\frac{Ub-Lb}{Ub^{rD} - LB^{rD}}.x_i^{rD}(\mathrm{t})) \tag{23}$$

In the exploitation phase, two individuals x_{rando1} and x_{rando2}, along with the best solution x_{best} identified so far, are used in the GQI process to generate the interpolation minimizer $x_{\min\_best,rando1,rando2}$ as Eq.(22). This point is expected to yield a better solution than those obtained from three randomly selected individuals.

To further enhance local exploitation, the position of the i^{th} individual is updated by searching around $x_{\min\_best,rand1,rand2}$, using a random perturbation $\mathrm{x_i}^{\mathrm{rD}}$, as defined in Eq. (23).

Finally, the i^{th} individual's position is updated based on a fitness comparison, as follows:

$$x_i(\mathrm{t}+1) = \begin{cases} x_i(\mathrm{t}) & fit(x_\mathrm{i}(\mathrm{t}) \le fit(v_\mathrm{i}(\mathrm{t}+1)) \\ v_i(\mathrm{t}+1) & fit(x_\mathrm{i}(\mathrm{t}) > fit(v_\mathrm{i}(\mathrm{t}+1)) \end{cases} \tag{24}$$

3.3. Application of QIOM to optimize the operating cost of MG system

The QIOM-based framework minimizes the daily operating cost of the MG shown in Fig. 1. Section 2 describes the system configuration, including power components, load demand, and electricity tariff. Renewable power generation is estimated using input data including solar irradiance, ambient temperature, and wind speed, as illustrated in Fig. 3 and Fig. 4. The implementation procedure follows the flowchart in Fig. 5.

https://doi.org/10.31436/iiumej.v27i3.4187

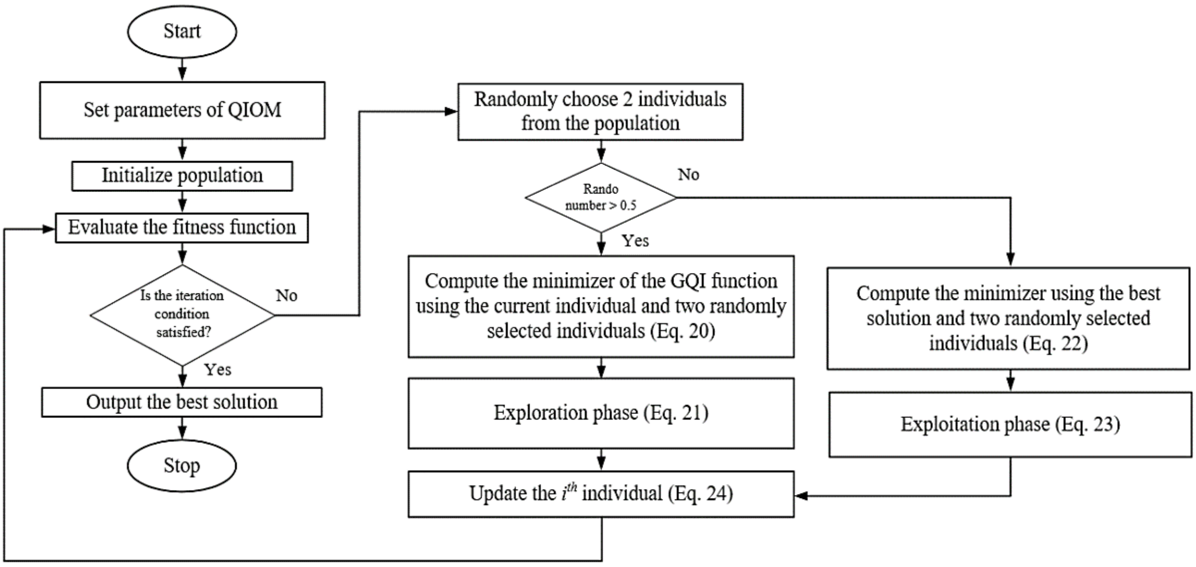

Figure 5. Flowchart of the QIOM algorithm for MG cost optimization.

The main steps are outlined as follows:

- **Step 1**: Define MG parameters

The optimization problem is formulated by specifying decision variables, constraints, and the objective function in Eq. (12). The algorithm is run for up to 500 iterations with a population size of 50. The decision variables are the hourly outputs of the DG, $P_{DG}(t)$, and the BESS, $P_{BESS}(t)$, over a 24-hour horizon. This results in 48 variables.

The PV and WT outputs are treated as fixed inputs and are obtained directly from the data. Other variables are derived through system equations and constraints. In particular, the power exchanged with the grid is computed using the balance equation in Eq. (11). The battery state of charge (SOC) is updated sequentially based on Eq. (7).

- **Step 2**: Initialize population

A randomly generated initial population of 50 individuals is created.

- **Step 3**: Evaluate initial population

The fitness value of each individual x_i *(where* $i=1\div50$*)* is calculated. The best solution obtained so far, x_{best} , is then identified, representing the selected values of P_{BESS} and P_{DG}.

- **Step 4**: Check the iteration conditions

If the stopping criterion is satisfied, the algorithm terminates. Otherwise, it continues to the next iteration

- **Step 5**: Perform optimization iterations

Each individual is updated based on a probabilistic rule. If *rando*>0.5, exploration is carried out using three randomly selected individuals Eq. (20) and Eq. (21). Otherwise, the exploitation phase is performed using the current best solution together with two random individuals, as described in Eq. (22) and Eq. (23).

- **Step 6**: Update best individual positions

Update the individuals' positions using Eq. (24). Reevaluate fitness to determine whether a better solution is found.

https://doi.org/10.31436/iiumej.v27i3.4187

The procedure repeats until the stopping condition is met. The final output includes the minimum operating cost and the corresponding hourly dispatch of the DG and BESS.

4. RESULTS AND DISCUSSION

All simulations were conducted using MATLAB R2023a on a personal computer equipped with an Intel Core i7 processor (1.9 GHz), 16 GB RAM, and Windows 10 Pro. For consistency, all algorithms used the same parameter settings described in Section 3.3. The compared methods are QIOM, PSO, GSA, GWO, and HBO. Each scenario was simulated over a 24-hour period. Since the algorithms are stochastic, 20 independent runs were carried out for each method. The results are evaluated using standard statistical metrics, including the best, mean, and standard deviation of the objective function.

In addition, the Wilcoxon signed-rank test is applied at a significance level of 0.05 to assess statistical differences between the methods. The numerical results for different operating scenarios are summarized in Tables 3 and 4. The corresponding power profiles are shown in Figs. 6-9.

To further evaluate performance, QIOM is analyzed under three operating scenarios:

- Scenario 1: MG without DG and BESS;
- Scenario 2: MG with DG but without BESS;
- Scenario 3: MG with both DG and BESS.

Table 3. Grid energy exchange under different MG scenarios.

Scenarios	Grid energy import (kWh)	Grid energy export (kWh)
1	66,432	-1,465.80
2	48,088	-2,368.21
3	48,460	-2,815.29

Table 4. Cost components of the MG under different scenarios.

Scenarios	Grid purchase cost ($)	DG Operating cost ($)	BESS operating cost ($)	Grid selling revenue ($)	Total operating cost ($)	Cost difference (%) (vs. Scenario 3)
1	8,558.47	0	0	-85.31	8,473.16	5.53
2	5,338.77	3,366.31	0	-137.83	8,567.25	6.70
3	4,705.50	3,322.06	165.58	-163.85	8,029.29	0

4.1. Scenario 1: MG without DG and BESS

Scenario 1 represents the basic configuration without variable power generation or an energy storage system. Under these conditions, the MG relies entirely on renewable energy sources and grid exchange to meet demand. As illustrated in Fig. 6, the electricity output from renewable sources is insufficient most of the time, especially in the early morning and late evening.

In this scenario, electricity imports from the grid become the primary and most consistently high source of supply throughout the day. Around midday, solar power production increases and temporarily exceeds demand, resulting in a short export period. This surplus is limited and cannot be stored because the MG lacks a BESS.

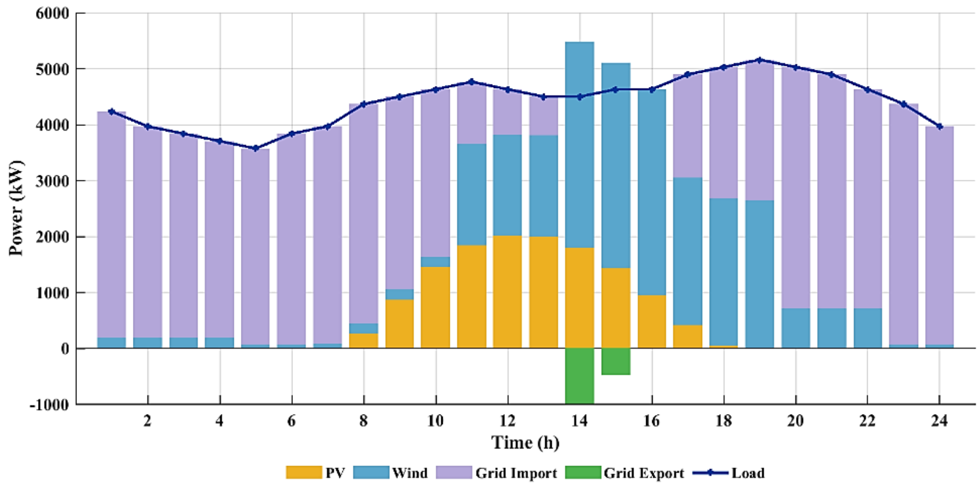

Figure 6. Hourly power distribution of the MG without DG and BESS.

Table 3 reflects this behavior: total energy imports reach 66,432 kWh, while energy exports remain minimal. The MG operates with continuous grid-based compensation. Operationally, the MG cannot regulate power or shift energy over time. The grid acts as the only adjustable supply source. This leads to inefficient use of available renewable energy sources when the time flexibility in energy use is not effectively exploited.

Table 4 clearly shows the economic impact. The cost of purchasing electricity from the utility grid constitutes the largest portion of the total operating cost, resulting in a total cost of $8,473.16. Although DG and BESS have no costs, the MG remains expensive because it relies on external power sources.

4.2. Scenario 2: MG with DG and without BESS

Compared to scenario 1, adding DG provides a controllable power source, shifting the system from fully reactive operation to partially controllable operation.

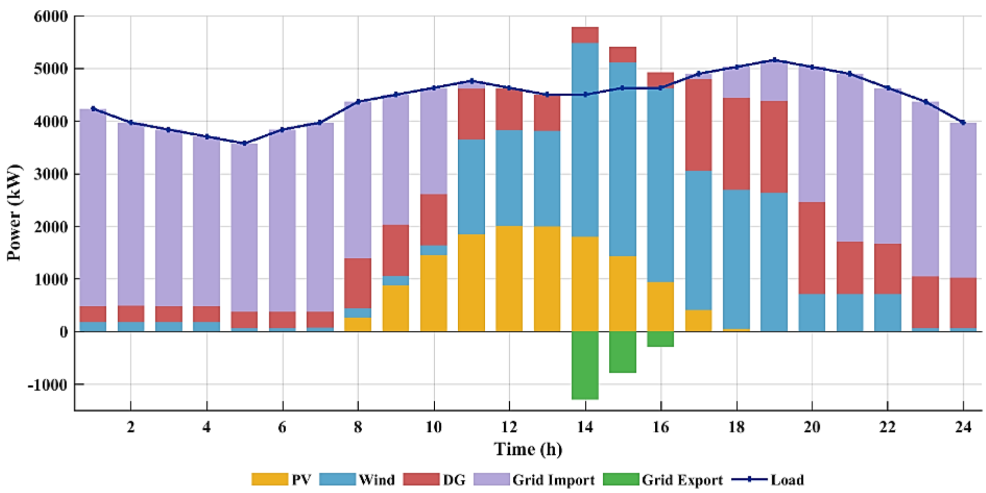

Figure 7. Hourly power distribution of the MG with DG and without BESS.

As illustrated in Fig. 7, DG is deployed during periods of insufficient renewable energy supply. This reduces the amount of electricity purchased from the grid, especially during medium- and peak-load periods. Grid electricity imports decreased to 48,088 kWh, representing a reduction of approximately 27.6% compared to Scenario 1.

From an operational perspective, DG acts as a deployable source that reduces real-time power imbalances but does not provide inter-temporal flexibility, which remains limited due to the lack of BESS. Excess renewable energy continues to be exported instead of stored, and energy cannot be shifted over time. This limitation is reflected in cost outcomes. Although electricity import costs from the grid decreased considerably to $5,338.77, the DG operating cost of $3,366.31 offset this benefit. As a result, total operating costs increased slightly to $8,567.25. Simply reducing electricity imports from the grid does not guarantee lower costs. Total costs depend not only on the amount of energy exchanged but also on the cost of local electricity production and the timing of energy use.

4.3. Scenario 3: MG with DG and BESS

Scenario 3 considers the coordinated operation of both DG and BESS, enabling both controllable power generation and energy storage. Fig. 8 shows a clear shift in operating strategy. BESS is charged during periods of surplus renewable energy generation and discharged during high-demand periods. This reduces the mismatch between power output and load demand.

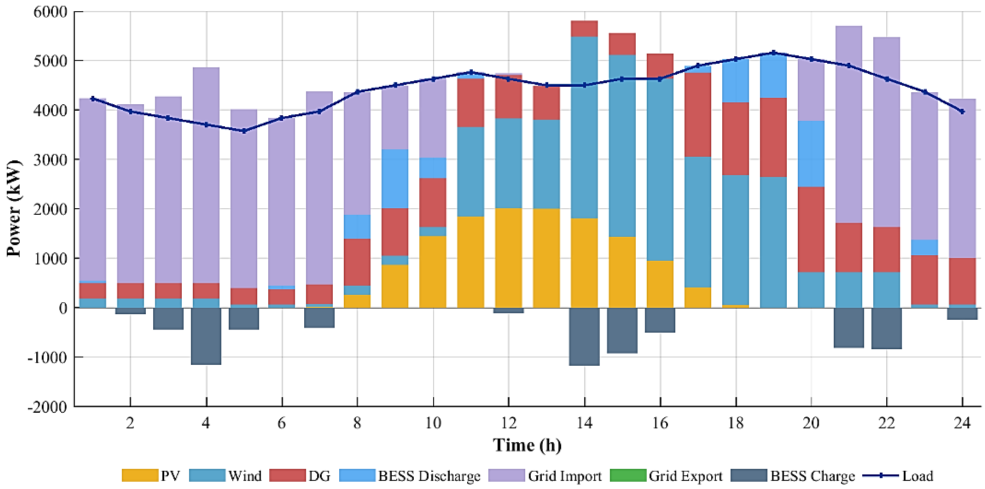

Figure 8. Hourly power distribution of the MG with DG and BESS.

Unlike previous scenarios, surplus renewable energy is not immediately exported but is partially stored for later use. During peak periods, the stored energy is released, reducing both electricity imports from the grid and the DG output.

As shown in Table 3, total energy imports (48,460 kWh) are similar to Scenario 2, but energy exports increase to 2,815.29 kWh, indicating improved utilization of renewable resources. Economically, grid electricity purchases decrease to $4,705.50. Although additional costs are incurred due to DG and BESS operation, these costs are offset by improved energy management and increased revenue from energy exports. Therefore, total operating costs decreased to $8,029.29, the lowest among all scenarios. Compared to Scenario 1 and Scenario 2, the cost reductions were approximately 5.53% and 6.70%, respectively. The results indicate that cost reduction is more closely related to the timing of energy exchange than to the total exchanged energy.

4.4. Comparative analysis of scenarios

Fig. 9 shows the power exchange between the MG and the utility grid in three scenarios and highlights the impact of DG and BESS on system operation.

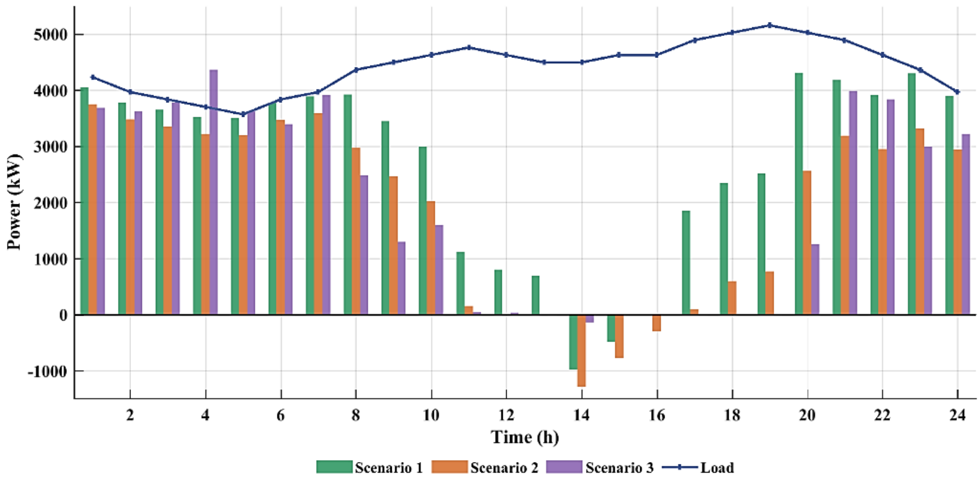

Figure 9. Power exchange between the MG and the utility grid under the three scenarios.

In Scenario 1, electricity imports from the grid predominate, with the grid acting as the primary balancing source. In Scenario 2, DG reduces the amount of electricity drawn from the grid. However, the overall model operates without an energy shift.

In Scenario 3, the grid exchange curve becomes smoother and less correlated with load. Peak-hour electricity imports decrease, and export timing is better controlled. This confirms the effectiveness of the BESS system, allowing for energy storage and redistribution over time.

Although the total amount of energy imported in Scenario 3 is equivalent to Scenario 2, the timing of energy exchange is substantially improved. This demonstrates that cost reduction depends not only on the amount of energy exchanged but also on the timing of the exchange, reflecting a decoupled relationship between energy quantity and economic cost. In this context, DG improves instantaneous power balancing, while BESS enables energy shifting over time; their combined operation enhances both system flexibility and economic efficiency.

4.5. Algorithm performance comparison

QIOM was compared with PSO, GSA, GWO, and HBO based on convergence performance, optimization accuracy, robustness, and computational efficiency. As shown in Fig. 10, QIOM rapidly decreased the objective function in the first few iterations and reached a stable region between iterations 150 and 200. This behavior reflects the algorithm's effectiveness in combining exploration with exploitation.

PSO converges faster initially but shows noticeable fluctuations, reflecting its sensitivity to random updates. GSA shows smoother convergence but at a slower rate, maintaining higher target values over a large number of iterations. GWO and HBO exhibit intermediate behavior, offering improved stability compared to PSO but converging more slowly than QIOM.

The statistical results in Table 5 further confirm these observations. Based on 20 independent runs, QIOM achieves the lowest best cost ($8,029.29) and the lowest mean cost ($8,091.60) among all compared algorithms. In addition, it achieves the lowest standard deviation (32.5), demonstrating better stability and robustness against random initialization. These results show that QIOM provides more consistent and reliable performance than the other methods.

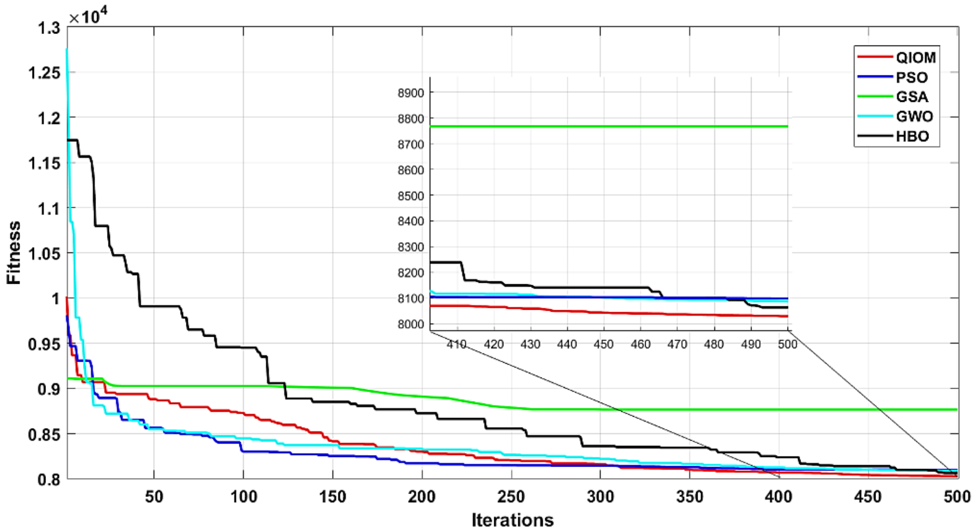

Figure 10. Convergence curves of the algorithms.

Table 5. Performance comparison of algorithms in terms of operating cost ($/day) over 20 independent runs.

Algorithm	Best	Time (s)	Mean	ΔMean (%)	Std	ΔStd (%)
QIOM	8029.29	47.22	8091.6	0	32.5	0
PSO	8098.55	5.23	8266.8	2.16	104.5	221.5
GSA	8766.96	10.32	8949.4	10.6	77.7	139.1
GWO	8087.38	6.32	8204.7	1.4	97.9	201.2
HBO	8063.62	5.94	8170.8	0.98	65.3	100.9

The box plot in Fig. 11 shows that QIOM produces a narrower distribution of results, confirming its stability compared to the other algorithms.

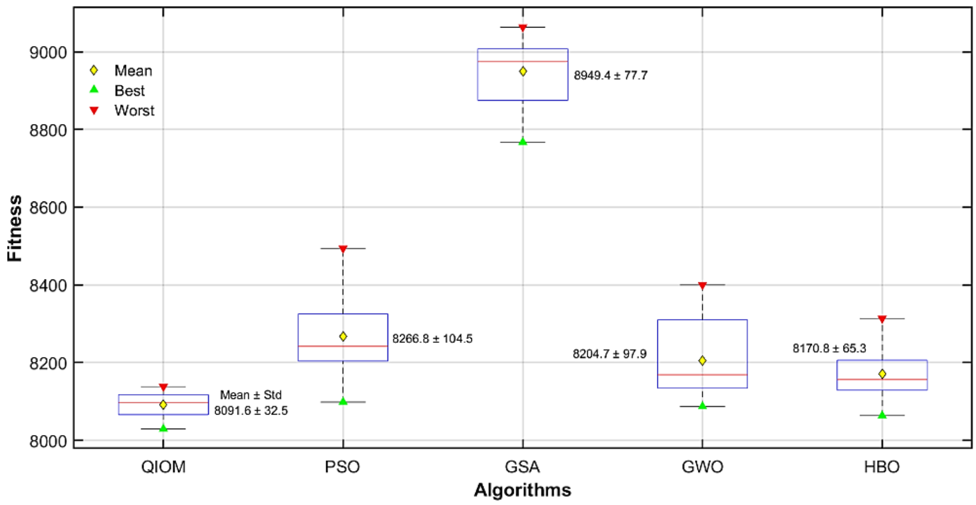

Figure 11. Boxplot comparison of fitness values over 20 independent runs.

To statistically validate QIOM's performance, the Wilcoxon signed-rank test results in Table 6 indicate that all observed differences are significant at the 0.05 level [38-40]. In particular, comparisons with PSO and GSA yield p-values below 0.001, highlighting QIOM's pronounced performance advantage.

Table 6. Wilcoxon signed-rank test results for algorithm comparison.

Comparison	p-value	Significance (α = 0.05)
QIOM vs PSO	< 0.001	Yes
QIOM vs GSA	< 0.001	Yes
QIOM vs GWO	0.002	Yes
QIOM vs HBO	0.015	Yes

In terms of computational time, QIOM requires more processing time due to its interpolation-based mechanism in a high-dimensional search space. However, the improved solution quality and stability make it suitable for offline optimization applications, where robustness is more critical than execution speed.

5. CONCLUSIONS

This study applies QIOM to minimize the operating cost of a grid-connected MG over a 24-hour scheduling horizon. The scenario analysis reveals different operational roles. The DG mainly supports real-time power balance. However, when used alone, it does not reduce costs. In contrast, the BESS introduces flexibility by shifting energy across time. This shifting effect improves the overall economic performance. The operating cost depends not only on the total energy exchanged with the grid, but also on when this exchange occurs. With coordinated operation (Scenario 3), the total cost is reduced by approximately 5.53% and 6.70% compared with Scenarios 1 and 2, respectively. In terms of optimization, QIOM yields lower costs than PSO, GSA, GWO, and HBO. The average cost is reduced by up to 2.16% compared to PSO and 10.6% compared to GSA. In addition, QIOM produces more stable results, as indicated by smaller variations across runs. The Wilcoxon signed-rank test further confirms that these improvements are statistically significant ($p < 0.05$). Although QIOM requires more computational time, it provides stable and high-quality solutions. Therefore, it is suitable for offline scheduling problems. Future research will consider uncertainty and real-time operation.

REFERENCES

[1] Akter A, et al. (2024) A review on microgrid optimization with meta-heuristic techniques: Scopes, trends and recommendation. Energy Strategy Reviews, 51:101298.

[2] Shaker HK, Keshta HE, Mosa MA, Ali AA. (2023) Adaptive nonlinear controllers based approach to improve the frequency control of multi islanded interconnected microgrids. Energy Reports, 9:5230-5245.

[3] Emam AA, Keshta HE, Mosa MA, Ali AA. (2023) Bi-level energy management system for optimal real time operation of grid tied multi-nanogrids. Electric Power Systems Research, 214:108957.

[4] Hassaballah EG, Keshta HE, Abdel-Latif KM, Ali AA. (2024) A novel strategy for real-time optimal scheduling of grid-tied microgrid considering load management and uncertainties. Energy, 299:131419.

[5] Tang Z, Liang T, Mi D, Huang Z, Jing Y, Wu H. (2026) Multi-objective optimization of virtual power plant with mobile storage considering renewable energy uncertainty and multiple flexible loads. International Journal of Electrical Power & Energy Systems, 143:108422.

[6] Halev A, Liu Y, Liu X. (2024) Microgrid control under uncertainty. Engineering Applications of Artificial Intelligence, 138:109360.

[7] Wang C, Zhang Z, Abedinia O, Gholami S. (2020) Modeling and analysis of a microgrid considering the uncertainty in renewable energy resources, energy storage systems and demand management in electrical retail market. Journal of Energy Storage, 33:102111.

[8] Shayeghi H, Davoudkhani IF. (2025) Uncertainty aware energy management in microgrids with integrated electric bicycle charging stations and green certificate market. Scientific Reports, 15:1-28.

[9] Yang M, Wang J, Chen Y, Zeng Y, Su X. (2024) Data-driven robust optimization scheduling for microgrid day-ahead to intra-day operations based on renewable energy interval prediction. Energy, 313:134058.

[10] Aguilar D, Quinones JJ, Pineda LR, Ostanek J, Castillo L. (2024) Optimal scheduling of renewable energy microgrids: A robust multi-objective approach with machine learning-based probabilistic forecasting. Applied Energy, 369:123548.

[11] Li Q, Zhang N, Zhu X, Liu J. (2021) Optimization of dynamic reactive power devices' coordinate operation for minimizing HVDC's successive commutation failure based on PSO. Journal of Engineering Research, 10(4):234-251.

[12] Hwang H, Shi S, Liang X, Zhang D, Dai W, Liu H. (2022) Optimal energy scheduling of grid-connected microgrids with demand side response considering uncertainty. Applied Energy, 327:120094.

[13] Zishan F, Akbari E, Montoya OD, Giral-Ramírez DA, Molina-Cabrera A. (2022) Efficient PID control design for frequency regulation in an independent microgrid based on the hybrid PSO-GSA algorithm. Electronics, 11(23):3886.

[14] Pervez I, Sarwar A, Tayyab M, Sarfraz M. (2019) Gravitational Search Algorithm (GSA) based Maximum Power Point Tracking in a Solar PV based Generation System. Innovations in Power and Advanced Computing Technologies (i-PACT), 1-6.

[15] Lazreg M, Benamrane N. (2022) Hybrid system for optimizing the robot mobile navigation using ANFIS and PSO. Robotics and Autonomous Systems, 153:104114.

[16] Amrane F, Gherouat O, Francois B, Itouchene H, Medani KBO, Chaiba A, Belkhier Y. (2025) Robust PSO-Optimized Power Control for Stand-Alone Variable-Speed DFIG Wind-Based High Stability and Power Quality Enhancement: Hardware Investigation-Based dSPACE1103. International Journal of Energy Research, 2025:2004125.

[17] Kumar G, Guerrero JM, Prakash O. (2021) Optimisation of solar / wind / bio-generator / diesel / battery based microgrids for rural areas: A PSO-GWO approach. Sustainable Cities and Society, 67:102723.

[18] Biabani F, Shojaee S, Hamzehei-javaran S. (2022) A new insight into metaheuristic optimization method using a hybrid of. Structures, 44:1168-1189.

[19] Devarapalli R, Rao BV, Al-durra A. (2022) Optimal parameter assessment of Solar Photovoltaic module equivalent circuit using a novel enhanced hybrid GWO-SCA algorithm. Energy Reports, 8:12282-12301.

[20] Itouchene H, Amrane F, Gherouat O, Boudries Z. (2025) Design and implementation of a grey wolf optimization – Based higher-order sliding mode controller for a DFIG-based wind turbine using dSPACE 1104. Energy Reports, 14:4324-4352.

[21] Salama D, Houssein EH, Said M, Oliva D, Nabil A. (2022) An Efficient Heap-Based Optimizer for Parameters Identification of Modified Photovoltaic Models. Ain Shams Engineering Journal, 13(5):101728.

[22] Shaheen AM, El-sehiemy RA, Hasanien HM, Ginidi AR. (2022) An improved heap optimization algorithm for efficient energy management based optimal power flow model. Energy, 250:123795.

[23] Abd M, El-said EMS, Elsheikh AH, Abdelaziz GB. (2022) Performance prediction of solar still with a high-frequency ultrasound waves atomizer using random vector functional link / heap-based optimizer. Advances in Engineering Software, 170:103142.

[24] Zhao W, Wang L, Zhang Z, Mirjalili S, Khodadadi N, Ge Q. (2023) Quadratic Interpolation Optimization (QIO): A new optimization algorithm based on generalized quadratic

interpolation and its applications to real-world engineering problems. Computer Methods in Applied Mechanics and Engineering, 417:116446.

[25] Du J, et al. (2024) A multi-objective robust dispatch strategy for renewable energy microgrids considering multiple uncertainties. Sustainable Cities and Society, 116:105918.

[26] Qing K, Du Y, Huang Q, Duan C, Hu W. (2024) Energy scheduling for microgrids with renewable energy sources considering an adjustable convex hull based uncertainty set. Renewable Energy, 220:119611.

[27] Otieno E, Farzaneh H. (2026) Multi-objective optimal sizing and location of the grid-connected renewable microgrids, considering cost-effectiveness, power loss, and network stability approaches. Energy Conversion and Management: X, 29:101465.

[28] Tutiempo Network. (2024) Temperature. https://en.tutiempo.net/ho-chi-minh-city.html

[29] Windfinder Network. (2024) Wind speed. https://www.windfinder.com/forecast/ho_chi_minh_city

[30] Keshta HE, Saied EM, Malik OP, Bendary FM, Ali AA. (2021) Fuzzy PI controller-based model reference adaptive control for voltage control of two connected microgrids. IET Generation, Transmission & Distribution, 15(4):602-618.

[31] Akter A, et al. (2024) A review on microgrid optimization with meta-heuristic techniques: Scopes, trends and recommendation. Energy Strategy Reviews, 51:101298.

[32] Taha MS, Abdeltawab HH, Mohamed YARI. (2018) An online energy management system for a grid-connected hybrid energy source. IEEE Journal of Emerging and Selected Topics in Power Electronics, 6(4):2015-2030.

[33] Babaei M, Azizi E, Beheshti MT, Hadian M. (2020) Data-Driven load management of stand-alone residential buildings including renewable resources, energy storage system, and electric vehicle. Journal of Energy Storage, 28:101221.

[34] Abujarad SY, Mustafa MW, Jamian JJ. (2017) Recent approaches of unit commitment in the presence of intermittent renewable energy resources: A review. Renewable and Sustainable Energy Reviews, 70:215-223.

[35] Garcia-Torres F, Bordons C. (2015) Optimal Economical Schedule of Hydrogen-Based Microgrids With Hybrid Storage Using Model Predictive Control. IEEE Transactions on Industrial Electronics, 62(8):5195-5207.

[36] Dao F, Zeng Y, Zou Y, Qian J. (2024) Fault diagnosis method for hydropower unit via the incorporation of chaotic quadratic interpolation optimized deep learning model. Measurement, 237:115199.

[37] Tong W, Su B, Zhan Y. (2026) An initial value insensitive method for phase equilibrium calculation: Constrained quadratic interpolation optimization algorithm. Expert Systems with Applications, 298:129597.

[38] Derrac J, García S, Molina D, Herrera F. (2011) A practical tutorial on the use of nonparametric statistical tests as a methodology for comparing evolutionary and swarm intelligence algorithms. Swarm and Evolutionary Computation, 1(1):3-18.

[39] Deng J, Zhang X, Jia X. (2025) Cost-efficient PON fault localization utilizing Wilcoxon signed rank test. Measurement, 256:118314.

[40] Zhang X, Feng R, Deng J, Jia X. (2026) An integrated scheme for fault detection and localization in passive optical network monitoring using the Wilcoxon signed-rank test. Results in Engineering, 29:109707.